# Can the water on deck influence the parametric roll of a FPSO? A numerical and experimental investigation

Marilena Greco[a,b,c,1], Claudio Lugni[a,b,c], Odd Magnus Faltinsen[b,c]

[a] *CNR-INSEAN, The Italian Ship Model Basin, via di Vallerano 139, 00128 Roma - Italy.*
[b] *Centre for Ships and Ocean Structures (CeSOS), NTNU, Trondheim - Norway.*
[c] *Centre for Autonomous Marine Operations and Systems (AMOS), Dept. of Marine Technology, NTNU, Trondheim - Norway.*

**Abstract**

Parametric roll and water on deck are investigated numerically and experimentally for a FPSO ship in head-sea regular waves in the zone of the first fundamental resonance. On the numerical side, a weakly-nonlinear potential seakeeping solver based on the weak-scatterer theory is coupled within a Domain-Decomposition (DD) strategy with a shallow-water approximation for water-shipping events and with a local analytical solution for bottom-slamming prediction. The comparison against the model tests confirmed the capability of the numerical method in predicting occurrence and features of parametric roll and water-on-deck phenomena. The solver has then been used to complement the physical analysis by examining the roll instability occurrence with a refined step of the calm-water roll natural frequency-to-excitation frequency ratio, $\omega_{4n0}/\omega$, around to 0.5. It is confirmed that the water shipping features are qualitatively and quantitatively affected by the parametric roll: the flow onto the deck becomes asymmetric and the water-on-deck occurrence becomes periodic with the roll-natural period, the level of green-water induced pressures increases. In some cases water shipping is even directly induced by large roll. In return the green-water loads affect the parametric instability by changing (both increasing and decreasing) the duration of the transient phase. This has been measured in terms of the variation of the time, $t_{max}$, required to reach the largest peak in the roll envelope before occurrence of steady-state conditions. The water on deck mostly increases the steady-state roll amplitude, $\xi_{4a}$, with an amount up to about seven degrees for the examined cases. Two scaling laws have been proposed for the variations of $t_{max}$ and $\xi_{4a}$ involving a modified steepness $\epsilon = (2A - f)/\lambda$, with $A$ and $\lambda$ the incident-wave amplitude and wavelength, respectively, and with $f$ the ship mean freeboard. The scaling laws $\alpha 1(\delta 1)$ and $\gamma 1(\delta 1)$ , with $\alpha 1 = -(\Delta t_{max}/T) \cdot \epsilon$, $\gamma 1 = -10\Delta\xi_{4a} \cdot \epsilon$, $\delta 1 = 100(\omega_{4n0}/\omega)^2 \cdot \epsilon$ and $T$ the incident-wave period, appeared to be more suitable in the region where water shipping is more relevant for parametric roll. They are well approximated by polynomial curves which could be useful to estimate the variations of $t_{max}$ and $\xi_{4a}$ due to water shipping for incident-wave parameters different from those examined here.

*Keywords:* Parametric roll, water on deck, experiments, domain-decomposition strategy, weak-scatterer theory, shallow-water.

*Corresponding author. Tel: +39 50299289; +47 73595440. E-mail address: marilena.greco@cnr.it; marilena.greco@ntnu.no.

## 1. Introduction

Parametric roll is a parametric resonance with instability behavior which may result in significant amplification of the roll motion (see *e.g.* [1]). This phenomenon has been documented as dangerous for different types of ships. For example, for large vessels like container ships it can lead to damage and loss of containers and cargo, for small fishing vessels it can cause the ship capsizing. The occurrence is connected with the time variation of the stability properties of the vessel due to changes in the restoring moment, and so in the transverse metacentric height $GM$. Such critical changes are supported by the interaction with incident waves sufficiently aligned with the vessel and nearly regular, *i.e.* with almost constant period and amplitude, and by sufficiently large heave and pitch motions. In such conditions, the level of ship roll damping is crucial in limiting the growing of the instability, the lower the damping the higher the possibility of parametric roll.

Finally there are ratios between the roll natural frequency and the encounter frequency, say $\omega_{4n}/\omega_e$, for which the instability occurs more easily. An uncoupled Mathieu-type instability analysis for the roll motion identifies $\omega_{4n}/\omega_e =$ 0.5,1, 1.5, and so on, as critical frequency ratios. In our case in general the vessel is a six degree-of-freedom (6-dof) system and the coupling among the motions could affect the actual occurrence of the phenomenon. However the values provided by the simplified analysis can be used to identify the frequency-ratio zones where parametric roll can occur more easily.

Here the case of a large Floating Production Storage and Offloading (FPSO) ship is examined. Such ships are used as platforms in oil industry, so they are typically at rest and weather-varying. Water on deck has been identified as dangerous for them in terms of operational limits while parametric-roll occurrence is not considered as an important factor. This could be due to the roll damping caused by the bilge keels and to the use of mooring-line systems. Recent water-on-deck experiments on a FPSO model without appendages and mooring systems and interacting with regular bow-sea waves highlighted the possible occurrence of parametric roll. So this platform is used here to examine more closely the parametric roll and the water on deck. Preliminary results of this investigation are documented in [2] but the numerical solver has been slightly improved since then. Moreover the present validation is more comprehensive and the analysis is more focused on the qualitative and quantitative mutual influence of parametric resonance and water shipping.

The FPSO model and the experimental set-up are described in the next section while the numerical solver chosen to confirm and complement the model tests is described in section 3. A physical investigation is carried out in section 4 with the attempt, among the others, to answer the key question of this work. Then the main results are summarized and the conclusions are drawn.

## 2. Experiments

A FPSO model in scale 1:40 has been tested in regular waves at the basin No. 2 (length x width x depth = 220 x 9 x 3.6 m) of CNR-INSEAN. The wave basin is equipped with a flap wavemaker Kempf & Remmers, hinged at a

height of 1.8 m from the bottom.

The main information of the model and the ship hydrostatic properties are given in the top-left table of figure 1, while the ship geometry is presented in the bottom sketch of the figure. In this study no bilge keels were used on the model and no hybrid technique was included to mimic the mooring-line action on the platform. The vessel was tested

| | |
|---|---|
| Length ($L$) | 4.22 m |
| Breadth | 0.81 m |
| Draft ($D$) | 0.25 m |
| Displacement | 663 kg |
| Metacentric height (GM) | 0.036 m |
| Pitch gyration radius ($K_{yy}$) | 0.27 $L$ |
| Roll gyration radius ($K_{xx}$) | 0.37 $B$ |

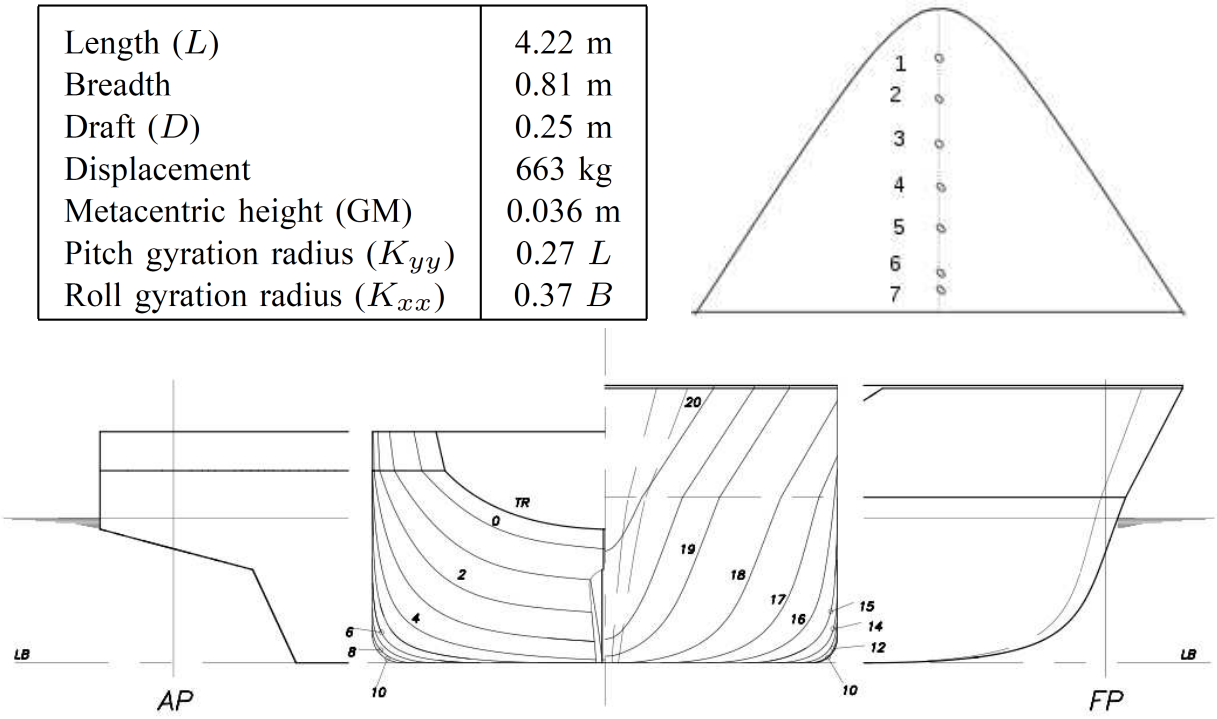


Figure 1: Experimental set-up. Top: main information of the ship model (left) and top view of the pressure sensors on the deck (right). Bottom: ship geometry.

in regular waves with heading angle of 180, 175 and 170 degrees to reproduce bow-sea waves coinciding or close to head-sea conditions, which are relevant for weather-varying platforms. The wavelength-to-ship length ratio $\lambda/L$ has been chosen as 0.75, 1, 1.25, 1.5 and 2, and the incident-wave steepness *kA* varied between 0.1 and 0.25 with step 0.05. The model was fixed to the carriage through a gimble and was examined as free to oscillate in (A) heave and pitch and in (B) heave, pitch and roll, while the remaining degrees of freedom were restrained.

Depending on the incident-wave parameters, the fluid-vessel interactions may lead to parametric-roll excitation, cause water-on-deck and bottom-slamming events, and result in high midship bending moments. The model was equipped in order to investigate globally and locally the possible effects of wave-vessel interactions. The rigid motions of the hull were measured with both an inertial (MOTAN) and an optical (Krypton) system to cross check the experimental conditions. The first one ensures a direct measurement of the rigid body vertical acceleration in the Center of Gravity (CoG), giving an estimation of the nonlinearities in the ship motions, the second one provides a good accuracy in the direct measurement of the ship motions. The ship model was split in two parts in the middle

and a three-cell balance was used to measure the mid-ship bending moment. The deck was without any barrier and limited by a vertical wall mimicking a deck house. Seven pressure sensors were distributed on the deck along the ship longitudinal axis as shown in the top-right sketch of figure 1, to quantify the green-water induced local loads. Four pressure sensors were placed along the keel to capture the occurrence of bottom-slamming events at 63, 158, 258 and 458 mm downstream of the ship section 19. The radiation and diffraction effects by the vessel were monitored through two wave-elevation sensors fixed to the ship model, respectively, at the front bow and at ship section 19. A third wave probe, fixed to the carriage, was placed around the longitudinal position of the CoG, at a transversal distance of approximately 3.5 m from the symmetric plane of the model.

With the aim to measure the undisturbed incident wave system, two wave probes were placed in front of the hull at a distance of approximately 5.7 and 34 m from the CoG, using a Kenek finger probe and a capacitance wire probe, respectively.

The behaviour in waves of the model was recorded using three cameras: a low-speed camera (with 25 fps) was used for the global 3D video recordings of the experiments, while two high-speed cameras (with 100 fps) provided top and front views of the ship deck in case of water shipping.

Because of the different dynamics of the local phenomena (water on deck and bottom slamming) from the global behaviour of the model (ship motions, global loads and incident waves) two different acquisition systems recorded the time histories of the several quantities. A high sample rate (10 kHz) acquisition system is used to record the pressure probes on the deck and on the bottom of the model; a lower sample rate (333 Hz) acquisition system records the global quantities. A common starting signal allows their synchronization, as well as the one of the camera systems.

Although the large number of physical quantities monitored in the present experiments, here we focus on the global motion of the ship, being the emphasis on the occurrence of the parametric roll and on the influence of the water on deck.

Since the roll-damping level is in general important for the occurrence and steady-state amplitude of the parametric instability, preliminary free-decay tests in roll have been performed (see figure 2). This showed a calm-water 1-dof roll natural period $T_{4n0} = 2\pi/\omega_{4n0} \simeq 3.56$ s. In general, this can be affected by the coupling with other ship degrees of freedom, as well as by incident waves that can modify the roll restoring moment. Assuming a 1-dof roll motion equation, an equivalent linear damping has been identified as $B_{44,1}/(I_{44} + A_{44}) = 0.03\ \mathrm{s}^{-1}$ corresponding to $B_{44,1} \simeq 0.0262 B_{44,cr}$, with $B_{44,cr}$ the critical damping. It means a small damping with limited effects on the roll, as confirmed by the investigations in section 4. This damping level is relatively low if compared with practical values for FPSO ships which typically range between 0.05 and 0.15. This is because here the damping is given by the wave-radiation and viscous bare-hull contributions which appeared in the present case well approximated by a linear behavior in terms of the body velocity. Bilge keels and mooring lines, usually used for FPSOs would lead to higher damping in roll with nonlinear trend of the damping coefficient with respect to roll speed.

Here the physical investigation is focused on the occurrence and features of parametric roll and water shipping in head-sea conditions. So only the measurements relevant for the discussion are examined. The analysis of the others

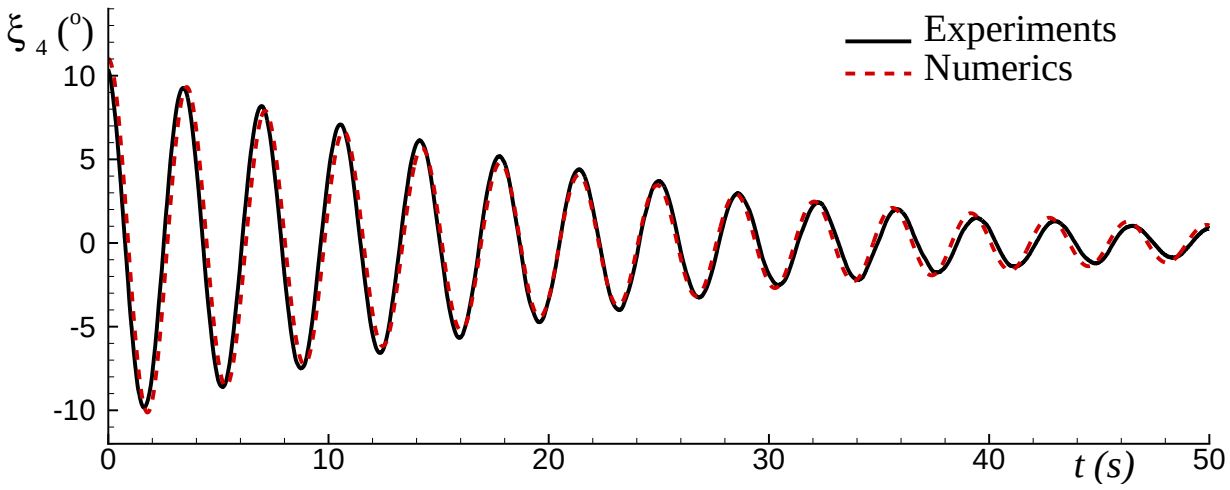


Figure 2: Free decay in roll from experiments and obtained numerically using linear damping identified from the model tests.

data is ongoing and will be considered in a future work. The wavelength-to-ship length ratios examined in the tests correspond to $\omega_{4n0}/\omega$ between about 0.4 and 0.66, $\omega$ being the incident-wave frequency. This implies a frequency range near and including the first fundamental resonance $\omega_{4n}/\omega$=0.5; the second resonance means $\omega_{4n}/\omega$=1 and is out of the study.

### 3. The numerical method

Numerically the seakeeping problem for a six degree-of-freedom ship possibly experiencing water shipping, bottom slamming and parametric instability is studied with a suitable Domain-Decomposition (DD) strategy described in detail in [3]. Here the main features, relevant to the discussion, are outlined. The solver couples a 3D weakly-nonlinear seakeeping potential-flow solver, with a local bottom-slamming solution and a water-on-deck model. The bottom slamming is handled through a local Wagner-type [4] solution and using an improved occurrence criterion which combines the Ochi's velocity criterion with a pressure condition, as proposed in [3]. The water shipping is solved assuming that only dam-breaking type of water on deck can occur. In practice this is one of the possible water-shipping scenarios but it also approximates well the global features of the most common water-on-deck scenario. The latter starts locally as a plunging wave hitting the ship deck near the front bow and then behaves as the flow developing after a dam break (see *e.g.* [5]). This means that the evolution of the shipped water can be studied within the shallow-water approximation. The problem is solved on a Cartesian grid fixed to the deck and using a splitting method to transform a 2D shallow-water problem in the deck plane into a sequence of 1D coupled problems along the main axes of the computational grid. In each direction, an exact Riemann solver is applied to estimate the variables fluxes and the coupled equations are stepped forward in time with a first-order scheme. The boundary conditions along the deck and possible superstructures are enforced using the level-set technique in [6] so to allow general deck-profile geometry immersed in the Cartesian grid.

The global wave-ship interaction solver is based on the weak-scatterer hypothesis (see e.g. [7]), assuming that incident waves and body motions are large relative to the scattering and radiation effects. This means the results are theoretically valid for wavelength-to-ship length ratio sufficiently large. Within this solution strategy, the impermeability body-boundary condition is satisfied averagely along the instantaneous wetted hull surface defined by the incident waves and the body motions. This leads to a correction of the scattering and radiation loads obtained from linear theory. Further, nonlinearities are retained up to the second order for Froude-Krylov and hydrostatic loads.

Because the problem involves nonlinear loads and anyway the transient phase must be investigated to detect parametric roll excitation, the equations of motions are solved in time domain using the approach in [8]. The rigid-body motion equations are written along a body-fixed coordinate system with origin in the center of gravity and read

$$\boldsymbol{M}\ddot{\boldsymbol{\xi}} + \boldsymbol{\Omega} \times \boldsymbol{M}\dot{\boldsymbol{\xi}} + \boldsymbol{A}_\infty \dot{\boldsymbol{\beta}} + \int_0^t \boldsymbol{K}(t-\tau)\boldsymbol{\beta}(\tau)\, d\tau = \boldsymbol{F}_{0\,\mathrm{nlin}} + \boldsymbol{F}_{h\,\mathrm{nlin}} + \boldsymbol{F}_{\mathrm{wod}} + \boldsymbol{F}_{\mathrm{slam}} \tag{1}$$

with $\boldsymbol{M}$ the ship generalized mass matrix, $\boldsymbol{\xi} \equiv (\xi_1, .., \xi_6)$ the six rigid degrees of freedom, $\boldsymbol{\Omega}$ the angular velocity vector $(\dot{\xi}_4, \dot{\xi}_5, \dot{\xi}_6)$ and the upper dots indicating time ($t$) derivatives performed along the instantaneous body axes. In equation (1), the cross product gives a six-component vector with first three components obtained through the cross-product of $\boldsymbol{\Omega}$ with the first three components of $\boldsymbol{M}\dot{\boldsymbol{\xi}}$ and the remaining components given by the cross-product of $\boldsymbol{\Omega}$ with the second three components of $\boldsymbol{M}\dot{\boldsymbol{\xi}}$. $\boldsymbol{A}_\infty$ is the infinite-frequency added-mass matrix and $\boldsymbol{K}$ is the retardation-function matrix. This equation system should be valid formally for linear problems in time domain but corrections due to nonlinear loads are included in the right-hand-side in the Froude-Krylov and hydrostatic loads, respectively, $\boldsymbol{F}_{0\,\mathrm{nlin}}$ and $\boldsymbol{F}_{h\,\mathrm{nlin}}$, and in the slamming and water-on-deck loads, respectively, $\boldsymbol{F}_{\mathrm{slam}}$ and $\boldsymbol{F}_{\mathrm{wod}}$, when such phenomena occur. A correction is also present in the added-mass and convolution-integral term of equation (1). Indeed, within linear theory, $\boldsymbol{\beta}(\tau)$ is a six-component vector equal to $\dot{\boldsymbol{\xi}}$ while here it is in general different and estimated in time from the body-boundary condition

$$V_n(\boldsymbol{x}, t) = (\boldsymbol{V}_{\mathrm{ship}} - \boldsymbol{V}_{\mathrm{wave}}) \cdot \boldsymbol{n}\,. \tag{2}$$

Here $V_n$ is the fluid-velocity component along the hull normal vector $\boldsymbol{n}$, $\boldsymbol{V}_{\mathrm{ship}}$ is the body velocity and $\boldsymbol{V}_{\mathrm{wave}}$ is the incoming-wave velocity. This implies that radiation and scattering phenomena are considered together. The solution strategy is as follows: $V_n$ is expressed in terms of $N$ prescribed basis functions $\psi_i$,

$$V_n(\boldsymbol{x}, t) = \sum_{i=1}^{i=N} \beta_i(t)\psi_i(\boldsymbol{x})\,, \tag{3}$$

with $\beta_i$ the $i$-th component of $\boldsymbol{\beta}$ (step 1); the resulting condition (2) is enforced through a Minimum Least-Square approach along the wetted hull defined by the incident waves and body motions (step 2); this provides the equations to find $\boldsymbol{\beta}$ (step 3). The procedure used follows the work in [7], but here $N$=6 is chosen (instead of $N$=5) and $\psi_i = n_i$ are adopted, with $n_i$ the $i$-th component of the generalized normal vector to the ship. In this way, the retardation function matrix $\boldsymbol{K}$ can be obtained from either the added-mass or the damping coefficients coming from solving the usual linear radiation problems.

In reproducing the experiments with the FPSO free only in heave, pitch and roll, in [2] the ship is taken as a 6-dof system and the fixed motions are simply set to zero, together with the possible effects of related hydrodynamic loads on the other motions. This is done considering the occurrence of reaction loads balancing inertial and hydrodynamic loads for the degrees of freedom kept fixed in the tests. The basis functions $\psi_i$ are kept to be six and so the vector $\boldsymbol{\beta}$ has six components. In the present work, the basis functions are estimated as six, *i.e.* consistently with a 6-dof system, but the coefficients $\beta_i$ connected with the restrained degrees of freedom are forced to be zero. This is done because, within the weak-scatterer assumption, as the wave steepness decreases (and so going toward linear conditions) the six components of $\boldsymbol{\beta}$ tend to become the time derivatives of the rigid motions, *i.e.* $\boldsymbol{\beta} \rightarrow \dot{\boldsymbol{\xi}}$. Therefore here the components of $\boldsymbol{\beta}$ that will correspond to the velocities of the fixed motions are enforced to be zero. This different strategy does not change significantly the results but slightly improves them, especially the pitch motion. Moreover, a close check of the results highlighted that using the original strategy the roll transient phase could be sensitive to the step adopted for the approximated evaluation in time of the retardation-function matrix. With the new approach this problem is avoided and the results appear so more reliable.

The obtained equations of motions are solved in time using a fourth-order Runge-Kutta scheme. When evolving from time $t$ to $t + \Delta t$ the water-on-deck loads, the slamming loads and the convolution integral terms, are estimated in $t$ and retained constant during the time interval $\Delta t$. The other loads are estimated at any time instant required by the scheme. The convolution integrals are evaluated by using a step-wise linear interpolation of $\boldsymbol{K}(t-\tau)$ and $\boldsymbol{\beta}(\tau)$ components and then integrating analytically. The integration accounts for the fact that the memory effects are limited, *i.e.* $\boldsymbol{K}(t-\tau)$ is non zero for a finite interval of time, so to limit the computational effort. The most time consuming element of the solver is represented by the water-on-deck solution, the related cost could be substantially reduced in the future by parallelizing this part. In the present implementation, overall the solver is efficient and can provide a time evolution of 400 periods in at most few hours on a modern computer.

One must note that this compound solver estimates only the wave-radiation potential-flow roll damping. Viscous damping corrections can be modelled introducing empirical coefficients in the equation of motion. In the present test case a linear damping coefficient is suitable and was estimated from the free-decay tests, as discussed in section 2. In the following the computations are performed both without and with the correction from the experiments so to check the effect of the viscous damping.

## 4. Physical investigation

Here model tests and numerical method are used to examine the parametric-roll and water-on-deck phenomena in head-sea conditions. It means that not all experimental conditions and not all measured variables are discussed, as for instance bottom pressure and mid-ship bending moment. They represent important sources of information for the wave induced loads on the vessel and their analysis is left for future work.

The head-sea experiments carried out at CNR-INSEAN highlighted parametric-roll instability in the zone of first

fundamental resonance for the vessel free in heave, pitch and roll (see the example in figure 3). The cause of the

Figure 3: CNR-INSEAN model tests on a FPSO model in regular head-sea waves. Front (top) and side (bottom) views showing the parametric-roll and water-on-deck occurrences. Time increases from left to right.

asymmetric motion in longitudinal waves on a vessel with port-starboard symmetry is the time variation with the encounter-wave frequency $\omega_e$ (in our case equal to $\omega$) of the roll restoring moment induced by the interaction with the incident waves and by sufficiently large vertical motion of the ship. The oscillations can lead to the change in sign of the transverse metacentric height and to the instability of the vessel. This results in the growing in time of the roll motion oscillating at its natural frequency $\omega_{4n}$, so we have instability and resonance at the same time.

The ship also experienced water on deck, which occurs if the relative motion is higher than the local instantaneous freeboard along the vessel. This is the result of wave-body interactions and, as we will see, can be induced by the vertical symmetric motions, *i.e.* heave and pitch, or by large parametric-roll oscillations. In both cases, one can expect that the occurrence of parametric-roll resonance affects the water shipping. For example the water flow along the deck will be not symmetric, as indicated by the snapshots in figure 3. Less clear is the influence of water-on-deck events on the parametric roll. These aspects will be examined in the following.

### *4.1. Numerical and experimental analysis of parametric roll and water on deck within the model test matrix*

Left part of table 1 examines the experimental occurrence of parametric roll in steady-state conditions and identifies $\lambda/L = 0.75$ and 1 as the wavelength-to-ship length ratios responsible for the instability. They correspond, respectively, to $\omega_{4n0}/\omega \simeq 0.402$ and 0.464, both of them close and smaller than the frequency ratio at the first parametric resonance. Condition $\omega_{4n0}/\omega \simeq 0.519$ is closer to 0.5 but larger and does not lead to any instability. This

Table 1: Occurrence of parametric-roll resonance (PR, left) and water on deck (WOD, right) for the cases studied experimentally and reproduced numerically.

| $\lambda/L \rightarrow$ | 0.75 | 1.00 | 1.25 | 1.50 | 2.00 | 0.75 | 1.00 | 1.25 | 1.50 | 2.00 |
|---|---|---|---|---|---|---|---|---|---|---|
| $\omega_{4n0}/\omega \rightarrow$ | 0.402 | 0.464 | 0.519 | 0.568 | 0.656 | 0.402 | 0.464 | 0.519 | 0.568 | 0.656 |
| Method $kA$ | PR | | | | | WOD | | | | |
| Exper. 0.10 | NO | YES | NO | NO | NO | NO | NO | NO | NO | NO |
| Num1 0.10 | NO | YES | NO | NO | NO | NO | NO | NO | NO | NO |
| Num2 0.10 | NO | YES | NO | NO | NO | NO | NO | NO | NO | NO |
| Exper. 0.15 | NO | YES | NO | NO | NO | NO | NO | NI | NO | NO |
| Num1 0.15 | NO | YES | NO | NO | NO | NO | NI | NI | NO | NO |
| Num2 0.15 | NO | YES | NO | NO | NO | NO | NI | NI | NO | NO |
| Exper. 0.20 | YES | NO | NO | NO | X | YES* | YES | YES | YES | X |
| Num1 0.20 | YES | YES | NO | NO | X | YES* | YES | YES | YES | X |
| Num2 0.20 | YES | YES | NO | NO | X | YES* | YES | YES | YES | X |
| Exper. 0.25 | YES | NO | NO | NO | X | YES | YES | YES | YES | X |
| Num1 0.25 | YES | NO | NO | NO | X | YES | YES | YES | YES | X |
| Num2 0.25 | YES | NO | NO | NO | X | YES | YES | YES | YES | X |

means that, within the used range of steepnesses, the parametric-roll occurrence is more shifted toward lower values of the frequency ratio $\omega_{4n0}/\omega$, so shorter incident waves appear more dangerous. In the shorter wavelength case parametric roll occurs for sufficiently large incident-wave steepness while for $\lambda/L = 1$ it is associated to sufficiently small $kA$. This suggests that nonlinear wave-body interactions support the instability for $\lambda/L = 0.75$ and work against for $\lambda/L = 1$. Symbol 'X' in the table refers to cases not studied experimentally because dangerous and so not investigated numerically either.

The solver described in section 3 was applied to the FPSO ship tested in the basin and predicted a calm-water roll natural period very close to the experimental value, *i.e.* $T_{4n0} \simeq 3.54$ s. The related parametric-roll occurrences are also given in the table as Num1 and Num2 and refer, respectively, to modelling only the wave-radiation roll damping from the linear potential-flow solver and to accounting also for the viscous correction from the free-decay tests. In table 1, the case with $\lambda/L = 0.75$ and $kA = 0.2$ was not exactly reproduced in the model tests. When compared with the prescribed incident waves, the actual waves appeared to have a larger amplitude, somewhat changing in time, and slightly larger period. They are closer to regular waves with $\lambda/L = 0.757$ and $kA = 0.21$, as documented in figure 4. There, two experimental curves are shown corresponding to two time intervals of the physical evolution with a shift of forty incident-wave periods $T$. This gives an indication of the experimental error in reproducing regular waves in this case. One must note that the experimental curve corresponding to the later incident-wave evolution (dashed dot-dot line in the figure) could also be affected by wave reflections from the ship model.

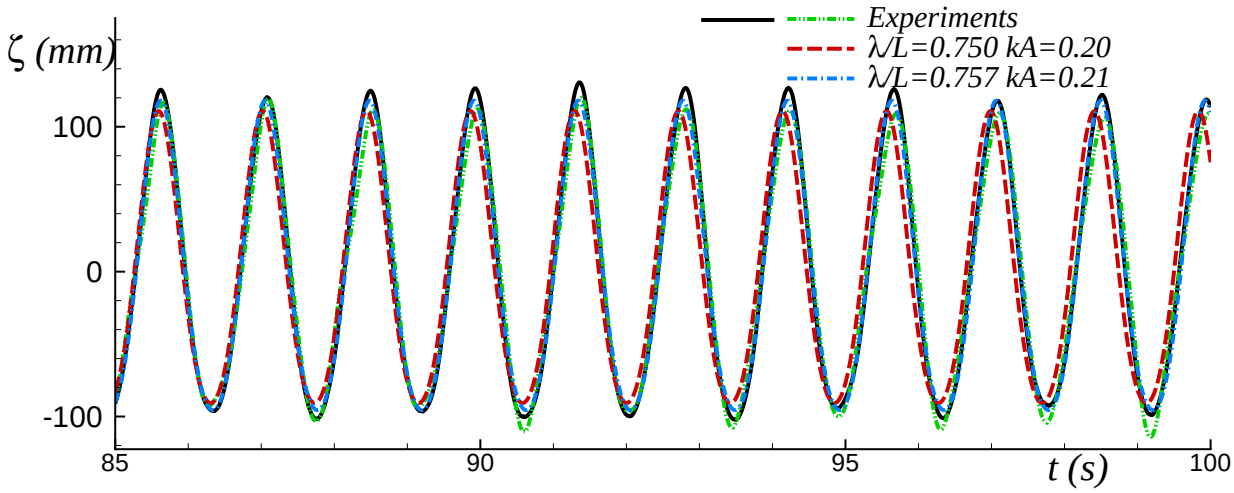


Figure 4: Experimental and numerical incident wave elevation for case with prescribed parameters: $\lambda/L$=0.75 and $kA$=0.2. Two experimental curves are shown (solid and dashed-dot-dot lines) corresponding to two time intervals of the physical evolution with a shift of forty incident-wave periods.

When $\lambda/L = 0.75$ and $kA = 0.2$ were used in the simulations the fully potential flow solution predicted a very slow instability and a roll amplitude still growing after $400T$ with a reached value of about six degrees. The solution with viscous damping did not capture any parametric roll. Using the more correct incident-wave conditions as input leads to parametric roll for both numerical solutions. Moreover, as discussed later, water shipping events induced directly by the parametric roll are predicted in agreement with the 3D video recordings. Both numerical solutions are globally consistent with the experimental data and confirm a limited effect of the viscous damping, due to its small level. A disagreement with the model tests is documented for the intermediate steepness $kA = 0.2$ with $\lambda/L = 1$. Experimentally no parametric roll was recorded while numerically the instability causes a steady-state roll amplitude $\xi_{4a} \simeq 8.4°$, which is more limited than for the other cases of parametric roll examined in detail later in the text. This suggests an incident-wave condition close to the limit of parametric-roll occurrence and a greater sensitivity of the instability excitation to the involved nonlinearities. So, on the numerical side, the results could have higher sensitivity to the approximations made in the solver. Another possible reason is connected with problems in reproducing accurately the prescribed incident waves by the wavemaker that was upgraded after this experimental campaign.

It is hard to investigate the close details of the parametric-roll excitation experimentally, because at the beginning the roll is very small and sensitive to the measurement errors. The numerical time histories show that in general the parametric roll develops after an initial phase where the roll evolution is characterized by both the incident-wave (excitation) frequency and the roll natural frequency. The duration and visibility of this stage depends obviously on the system tendency to instability; the higher is the tendency, the shorter and the less clear this stage becomes. An example is given in figure 5 for $\lambda/L = 1$. The case with steepness $kA = 0.1$ (top plot) shows clearly this initial phase, which is still present for the steeper condition (bottom plot) but with shorter duration (less than $5T$) and hidden by the

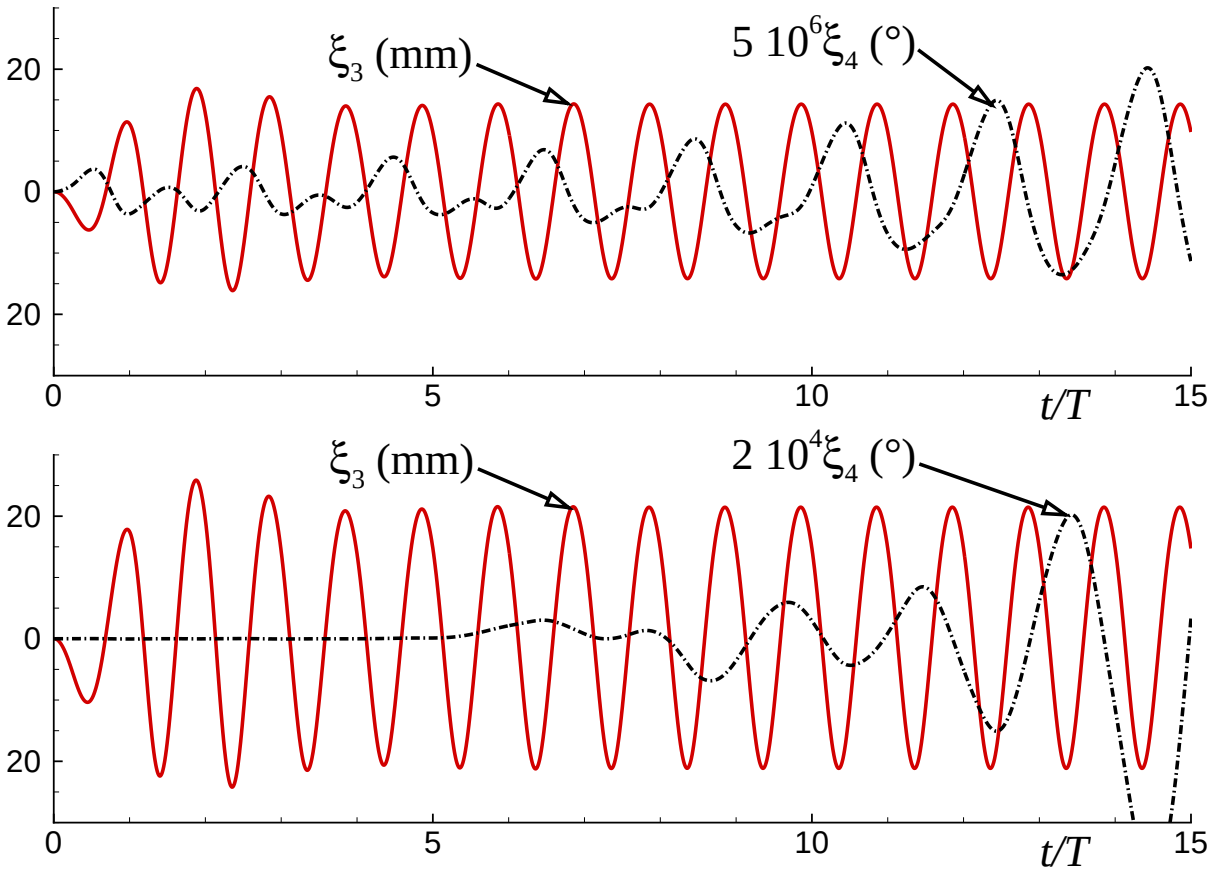


Figure 5: Initial transient phase for heave $\xi_3$ and roll $\xi_4$ motions for $\lambda/L$=1.00 with $kA$=0.1 (top) and with $kA$=0.15 (bottom). The results were obtained numerically with the solver described in section 3 using the viscous damping correction from the free-decay tests. $T$ is the incident-wave period.

rapid increase of the roll amplitude due to the instability.

The transient phase of the roll motion during the instability development is presented in figure 6. Here a synchronization process is used because in general the occurrence of parametric roll in time is different between experiments and numerics depending, for example, on the distance of the ship from the wavemaker. In particular the maximum peaks of $\xi_4$ for the experiments and for the numerics have been synchronized and set at about $100T$ in all conditions examined in the figure. The maximum peak can be in general larger or equal to the roll peaks in steady-state conditions; in the latter case it corresponds to the first peak in steady-state conditions. The cases examined are three of the four experimental cases with parametric roll; the fourth case (with $\lambda/L = 1$ and $kA = 0.1$) is documented in the left-center plot of figure 7. The roll evolution given by Num2 grows more slowly than the solution provided by Num1 and, except for $\lambda/L$=0.757 and $kA$=0.21, in all cases it increases more similarly to the experiments. After the maximum peak of the numerical $\xi_4$, an envelope is caused by the instability on the roll motion, as well as on the heave and pitch motions (not shown here). The amplitude of this envelope dies out in time much quicker for Num2 due to

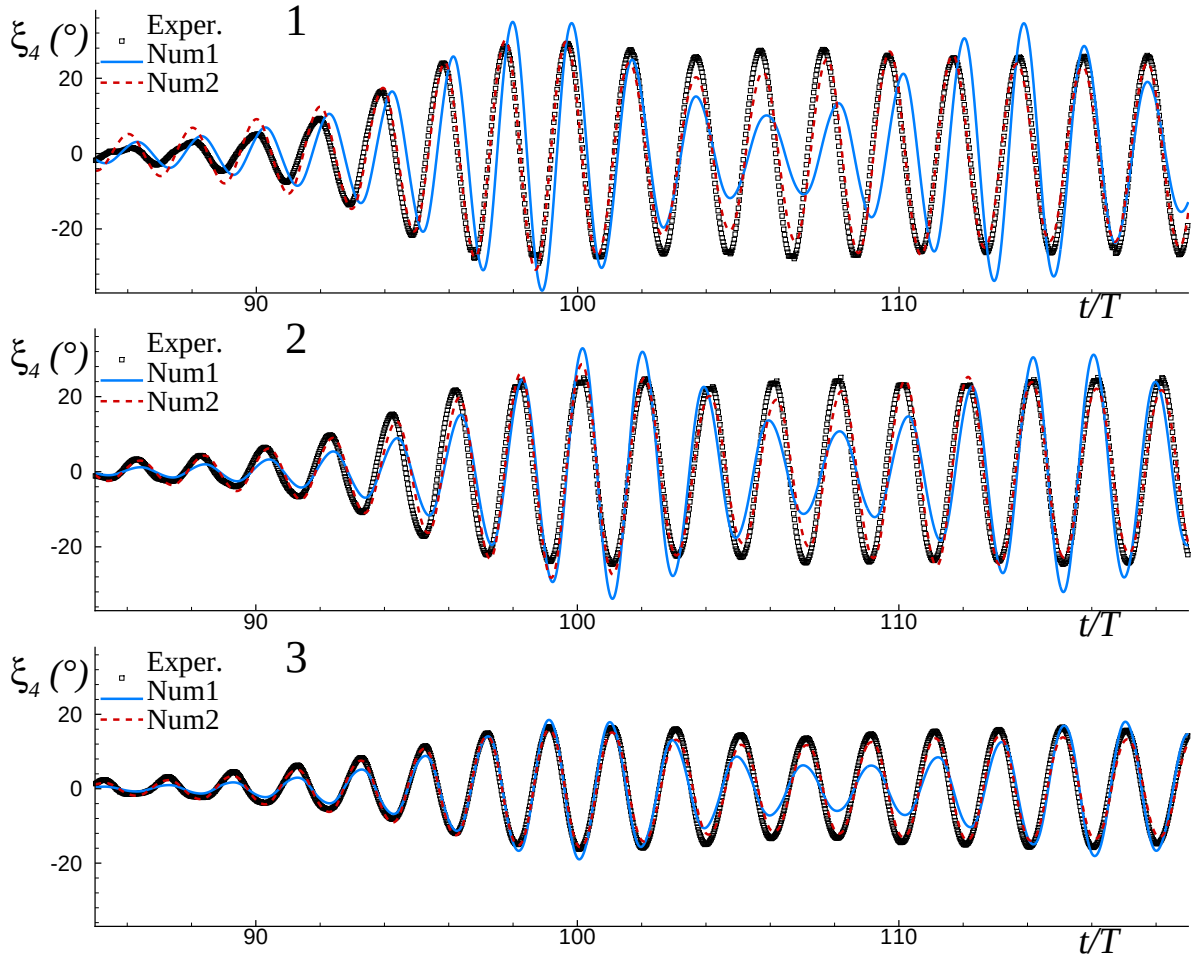


Figure 6: Parametric-roll occurrence: experimental and numerical transient phase of roll motion $\xi_4$ during the establishment of parametric roll. 1: $\lambda/L$=0.757 and $kA$=0.21; 2: $\lambda/L$=0.75 and $kA$=0.25; 3: $\lambda/L$=1 and $kA$=0.15.

the viscous damping and this is more consistent with the experimental time histories (check figure 6).

Almost steady-state conditions with parametric resonance are examined in figures 7 and 8 in terms of rigid ship motions measured experimentally and predicted with Num1 and Num2 solution strategies. Actually, as mentioned above, the results for incident waves with $\lambda/L$=1 and $kA$=0.1 (left of figure 7) refer to the transient stage during the occurrence of parametric roll. In this case experimentally the parametric roll occurs towards the end of the temporal window set for motion measurements. So the physical steady-state conditions are not available and we compared the transient phase of the motions during the parametric roll occurrence. For every wave case, to allow the comparison, one numerical motion from Num1 and Num2 simulations is synchronized with the experiments and the same shift is used for the other motions. Heave and pitch evolutions are dominated by the incident-wave period while the roll motion oscillates, with a longer period about 2.85 s, 2.86 s and 3.3 s going from the shortest to the longest incident-wave cases. This means that the roll-natural period is different from $T_{4n0}$ and in particular is smaller than the calm-water value for all cases. This suggests a variation of the roll natural period in waves, which depends on

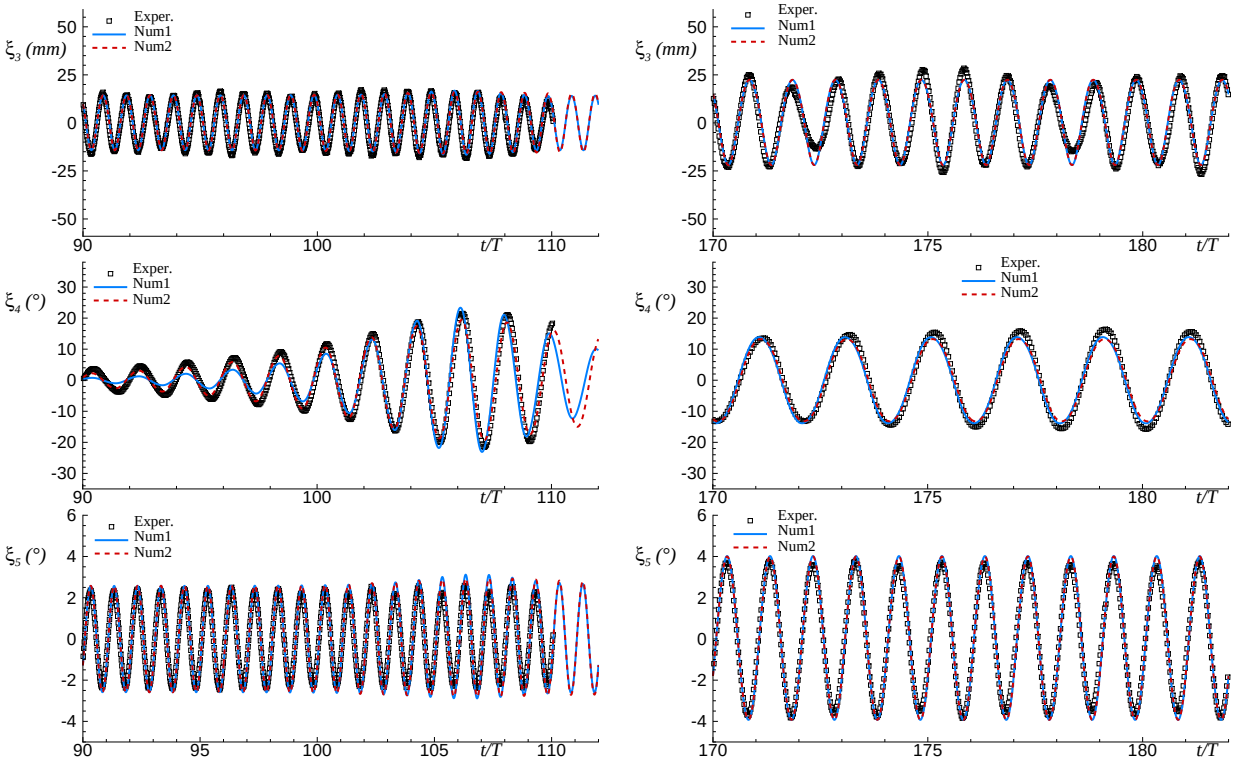


Figure 7: Parametric-roll occurrence: heave (top), roll (center) and pitch (bottom) motions for $\lambda/L$=1 with $kA$=0.1 (left) and with $kA$=0.15 (right). $\xi_3$=heave, $\xi_4$=roll, $\xi_5$=pitch. $\xi_3$ is given at the model scale.

the ratio $\lambda/L$ and on the involved wave-body interaction effects. $T_{4n}$ coincides with twice the incident-wave period, *i.e.* the condition for first fundamental resonance $\omega_{4n}/\omega = 0.5$ is satisfied. From present numerical studies, any time parametric roll occurs, the coupling between the motions and the nonlinear effects force in general the instantaneous $\omega_{4n}$ to change and tune itself to be $\omega_{4n} = \omega/2$.

In all incident-wave cases, the roll amplitude exceeds ten degrees, which is often the maximum allowed roll amplitude for a FPSO in normal operational conditions, and reaches almost thirty degrees in the worst case. One must note however that the examined ship is not equipped with bilge keels which would have provided much higher damping in roll. The two numerical solutions are very similar because the viscous damping for the studied ship configuration is small and agree quantitatively well with the experiments in terms of ship motions. This means that the fully potential-flow solution could be used to reproduce the experiments. However, for a more realistic FPSO model with bilge keels a proper estimation of the viscous roll damping is needed to predict correctly the roll motion. Simplified methods could be used to quantify the bilge-keel effects such as the Ikeda method (see *e.g.* in [9]) or as proposed for instance in [10].

The largest differences between numerics and experiments occur for heave and pitch, especially for the shorter waves. This is consistent with the fact that the method is based on the weak-scatterer hypothesis (see section 3). On the other hand, the physical heave and pitch do not appear smooth everywhere and indicate the presence of a

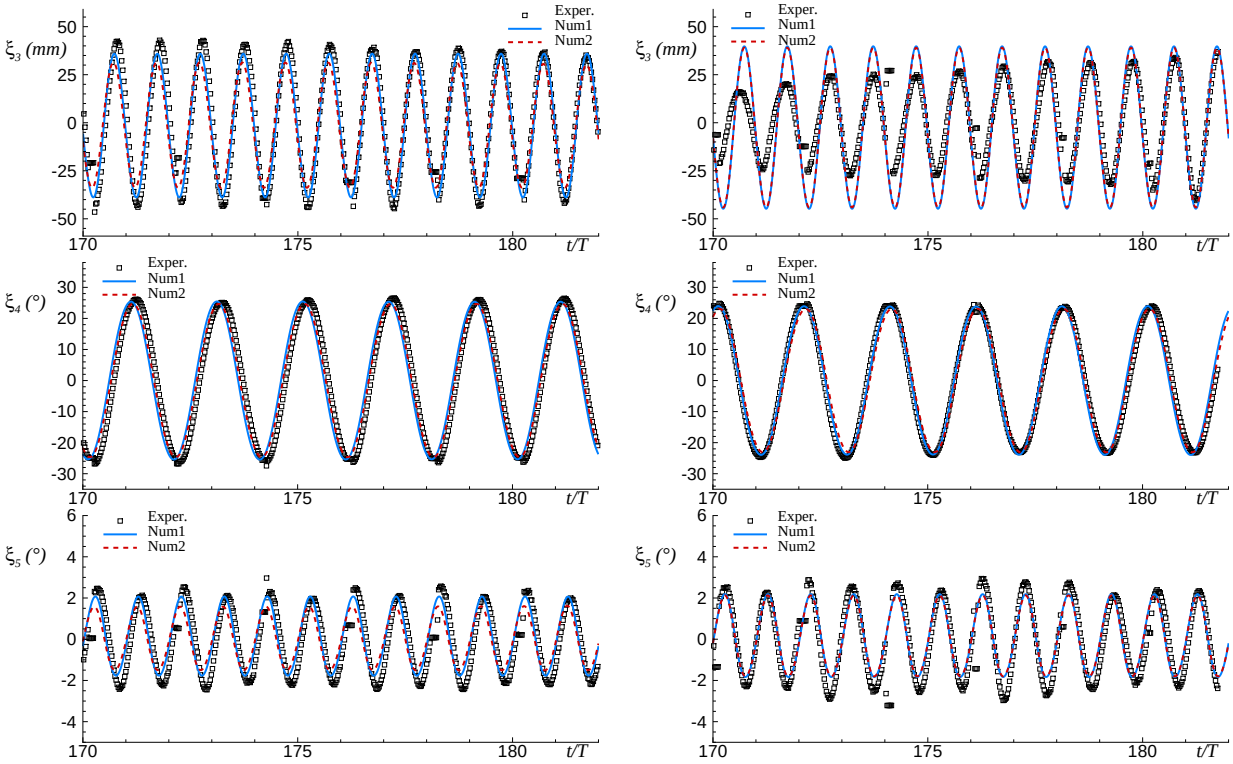


Figure 8: Parametric-roll occurrence: heave (top), roll (center) and pitch (bottom) motions for $\lambda/L$=0.757 and $kA$=0.21 (left, corresponding to prescribed incident waves with $\lambda/L$=0.75 and $kA$=0.2 in the model tests) and for $\lambda/L$=0.75 and $kA$=0.25 (right). $\xi_3$=heave, $\xi_4$=roll, $\xi_5$=pitch. $\xi_3$ is given at the model scale.

low-frequency component. Checking the whole available time histories of the experiments, this envelope tends to disappear in time but it is not connected with the parametric roll because it appears earlier than the roll instability. The fully potential-flow solution seems to be somewhat closer to the experiments for the heave and pitch evolutions but this could be just by chance. The use of the viscous-damping correction in the simulations gives a tiny better agreement in phasing of the steady-state roll time histories with the model tests for all the cases, in addition to the transient-phase improvement previously discussed.

Right part of table 1 examines the experimental and numerical occurrence of water on deck in steady-state conditions for the incident waves examined in the model tests. The boolean value 'NI' indicates very limited amount of shipped water qualitatively recorded by the experimental videos. Numerically it means water on deck associated with less than 0.4 dm$^3$ as maximum volume of shipped liquid per event. This corresponds to an average maximum water level on the deck less than 2 mm at model scale. From the global comparison, the two numerical solutions show the same results and agree with the model tests except for the case with $\lambda/L = 1.00$ and $kA = 0.15$. This is at the limit of water on deck occurrence both as predicted numerically and observed from the videos. This suggests a certain sensitivity of the numerical solution to the used approximations of the nonlinear effects. The wave-ship interaction for prescribed incident waves with $\lambda/L = 0.75$ and $kA = 0.2$ represents an interesting case. If these parameters are given

as input for the numerics including viscous damping, then neither water shipping nor roll instability are predicted. When $\lambda/L = 0.757$ and $kA = 0.21$ are used (see discussion above), parametric roll occurs and is the responsible for water on deck as in the experiments. This fact is indicated by the symbol 'YES*' in the table and suggests that these

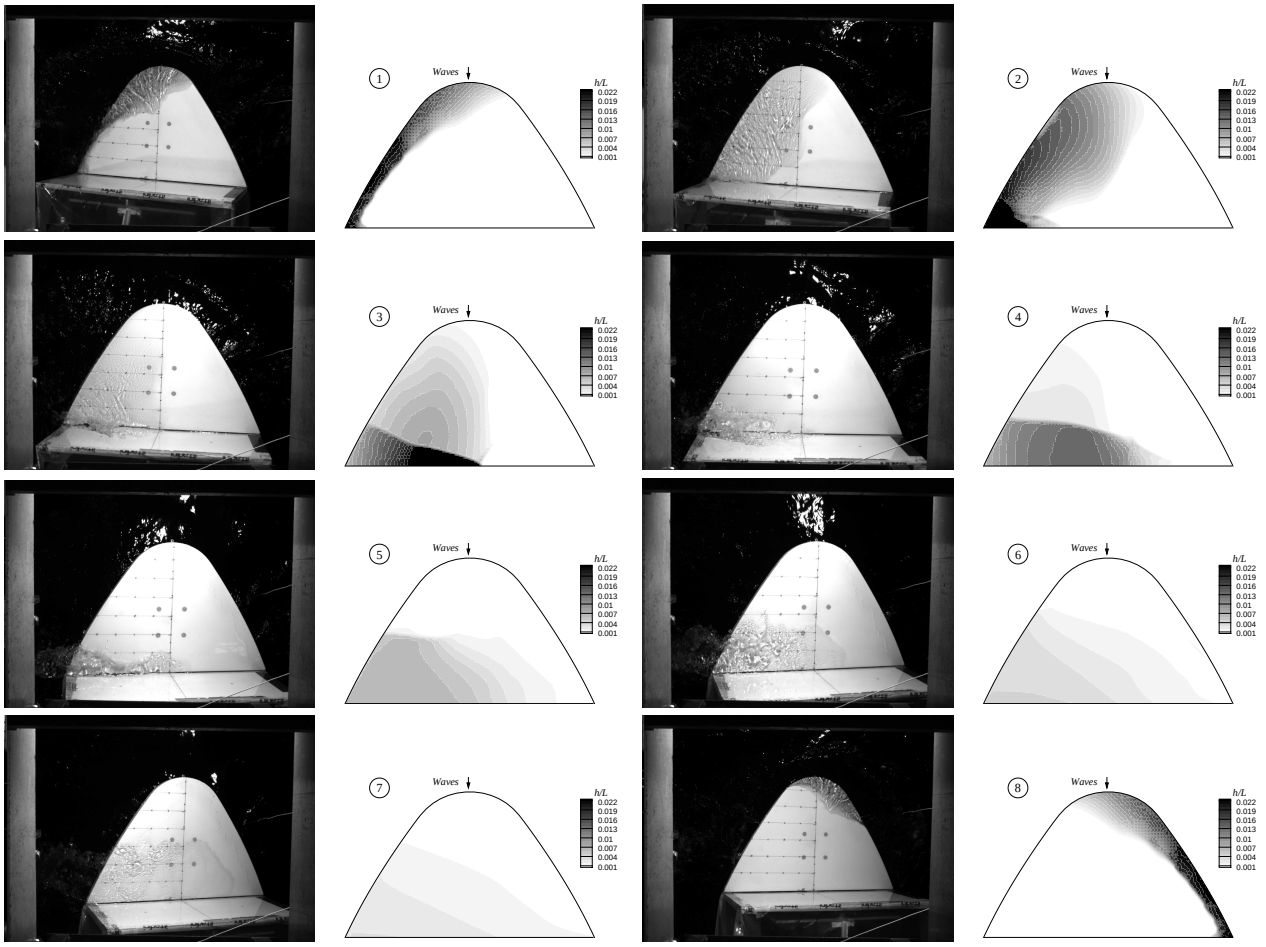


Figure 9: Water-on-deck occurrence: top view of the shipped water for waves with $\lambda/L$=0.75 and $kA$=0.25. In each panel: experiments (left) and Num2 (right). From left to right and from top to bottom: $t_0$, $t_0 + 0.1T$ , $t_0 + 0.2T$, $t_0 + 0.3T$, $t_0 + 0.4T$, $t_0 + 0.5T$, $t_0 + 0.6T$ and $t_0 + T$ with numerical $t_0 \simeq 170.34T$ and $T$ the incident wave period. The numerical deck is enclosed within a rectangular area discretized with $\Delta x = \Delta y \simeq 0.0008L$ and the used time step is $\Delta t = 0.005T$. $h$= water level on the deck.

incident wave parameters are close to the limit for occurrence of parametric roll, which is able to cause water shipping.

The case with $\lambda/L = 0.75$ and $kA = 0.25$ is used next to investigate more in detail the features of water shipping. These incident waves cause also parametric roll which is able to modify the features of the shipped liquid and the resulting green-water loads. The water on deck events are symmetric relative to the ship longitudinal axis until the parametric roll occurs and then are driven by the instability. This is documented by the top views of the deck in figure 9 during the steady-state conditions with established parametric resonance. The figure gives both snapshots from the high-speed cameras and the numerical solution Num2. From the two results, a water shipping begins from the left side of the front bow (panel 1 of the figure), the liquid closer to the front bow advances towards the vertical superstructure

(panel 2) while the water shipped near the wall tends to move towards the opposite side of the ship. The two masses of liquid eventually meet in the form of an impact with the superstructure and with accumulation of water rising along the wall (panel 3). Later on the water is reflected from the superstructure and starts to distribute along the deck and to reduce in time its level. At this stage a water-off-deck phase occurs at the side where the liquid entered the deck because it is closer to the reflected water (panels 4-7). After one incident-wave period a new water shipping starts from the opposite side of the deck (panel 8). It means that the parametric roll makes the water-on-deck events to become periodic with $T_{4n}$ instead of with the excitation period $T$.

While experiments and numerics are consistent qualitatively, it is hard to attempt a more quantitative comparison. This is because of the perspective angle of the video camera and because different water-on-deck events of the same experimental run indicated some local variations of the water flow on the deck (see in [2]). Such variations could be

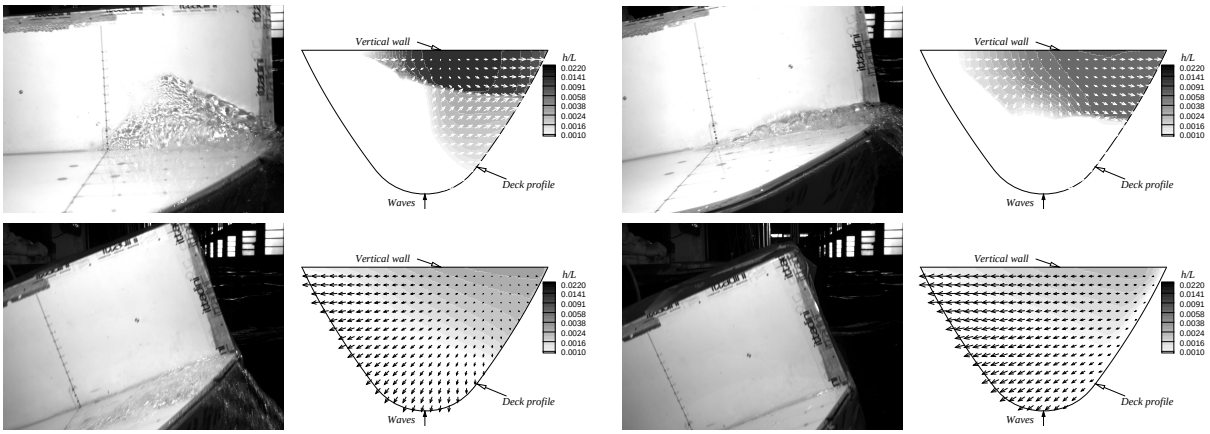


Figure 10: Water-off-deck phase near the superstructure for waves with $\lambda/L$=0.75 and $kA$=0.25. In each panel: front view from the experiments (left) and top view from the numerics (Num2) with velocity vectors of the shipped water (right). The vectors are white in the top plots and black in the bottom plots to make them more visible. From left to right and from top to bottom: $t_0+0.3T$ and $t_0+0.4T$, $t_0+0.6T$ and $t_0+0.7T$ with numerical $t_0 \simeq 170.34T$ and $T$ the incident wave period. The numerical deck is enclosed within a rectangular area discretized with $\Delta x = \Delta y \simeq 0.0008L$ and the used time step is $\Delta t = 0.005T$. $h$= water level on the deck.

the result of the low-frequency envelope, or not perfect steady-state conditions, detected in the ship motions for this case (see right part of figure 8).

The water-off-deck phase for this incident-wave case is examined in detail in figure 10 combining the numerical results with front-view video recordings from the experiments. The first three time instants shown correspond to those in panels 4, 5 and 7 of figure 9. In the first two time instants the experiments indicate clearly a water flux leaving the deck, this is reduced substantially at the third instant due to the increasing roll angle against water-off-deck and is over in the last snapshot. The same conditions of the water are confirmed by the simulations through the directions and the lengths (indicating the value) of the liquid velocity vectors.

*4.2. Extended numerical analysis of parametric roll and water on deck*

Due to the promising comparison with the experiments, the numerical method with roll-damping correction from the experiments (Num2) has been used to investigate more in detail the parametric roll occurrence and its interaction with possible water on deck events. The frequency ratio $\omega_{4n0}/\omega$ is varied between 0.38 and 0.51 with a step of 0.01 and the incident-wave steepness $kA$ is varied as done in the experiments.

The results in terms of parametric-roll occurrence are presented in table 2 and confirm that for the examined steepness range the instability tends to occur for $\omega_{4n0}/\omega$ smaller than 0.5. The case with 'NIYES' is characterized

Table 2: Occurrence of parametric-roll resonance for the cases studied numerically.

| $\lambda/L \rightarrow$ | 0.67 | 0.70 | 0.74 | 0.78 | 0.82 | 0.86 | 0.90 | 0.94 | 0.98 | 1.02 | 1.07 | 1.11 | 1.16 | 1.21 |
|---|---|---|---|---|---|---|---|---|---|---|---|---|---|---|
| $\omega_{4n0}/\omega \rightarrow$ | 0.38 | 0.39 | 0.40 | 0.41 | 0.42 | 0.43 | 0.44 | 0.45 | 0.46 | 0.47 | 0.48 | 0.49 | 0.50 | 0.51 |
| $kA$=0.10 | NO | NO | NO | NO | NO | NO | NO | YES | YES | YES | YES | YES | YES | NIYES |
| $kA$=0.15 | NO | NO | NO | NO | NO | YES | YES | YES | YES | YES | YES | NO | NO | NO |
| $kA$=0.20 | NO | NO | NO | YES | YES | YES | YES | YES | YES | YES | NO | NO | NO | NO |
| $kA$=0.25 | NO | YES | YES | YES | YES | YES | YES | YES | NO | NO | NO | NO | NO | NO |

by a very slow instability and with a steady-state amplitude less than three degrees. This indicates that for larger frequency ratios the parametric roll tends to disappear. It is also confirmed that larger steepness brings to instability for lower frequency ratio and out from instability otherwise. In any case the occurrence of the parametric resonance is limited within a certain range of $\omega_{4n0}/\omega$. This is reasonable because there is a limit for the variation of the roll-natural frequency so to tune to the first fundamental resonance.

The duration of the roll transient phase is examined in the left plot of figure 11 for the cases with parametric roll in terms of the time, $t_{max}$, required to reach the largest peak in the roll envelope before occurrence of steady-state conditions (see the definition in the right-bottom plot of later figure 12). The right plot of the figure examines the parametric-roll amplitude in steady-state conditions. From the results, as $kA$ increases the value of $\omega_{4n0}/\omega$ corresponding to the minimum transient phase reduces, *i.e.* shorter incident waves cause quicker the parametric roll. In general the parametric roll needs several incident-wave periods to reach steady-state conditions, the lowest value of $t_{max}$ predicted is around $60T$. $t_{max}/T$ enlarges both for sufficiently short and long incident waves, but the shorter waves are dangerous because they are associated with the largest steady-state roll amplitudes when parametric roll is excited (see right plot). It is confirmed that shorter waves can excite instability only if they are sufficiently steep otherwise the parametric roll occurrence moves toward $\omega_{4n0}/\omega = 0.5$. For each steepness the roll amplitude decreases almost linearly with the frequency ratio, while for a fixed $\omega_{4n0}/\omega$ the roll amplitude increases nearly linearly with reducing $kA$.

The occurrence of water on deck for the examined incident-wave cases is given in table 3. As expected longer waves are able to cause water on deck at lower steepnesses because they will be characterized by larger amplitudes than

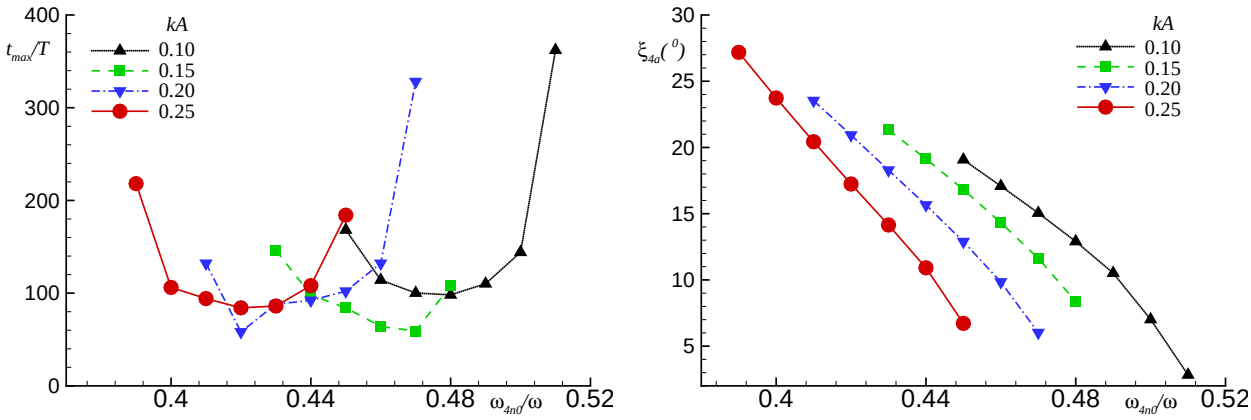


Figure 11: Features of parametric roll from numerical analysis: time required for the first roll peak (left) and steady-state roll amplitude (right) for each examined steepness $kA$ as a function of the ratio between the calm-water roll natural frequency and the incident-wave frequency, $\omega_{4n0}/\omega$. $T$ is the incident-wave period.

Table 3: Occurrence of water on deck for the cases studied numerically.

| $\lambda/L \rightarrow$ | 0.67 | 0.70 | 0.74 | 0.78 | 0.82 | 0.86 | 0.90 | 0.94 | 0.98 | 1.02 | 1.07 | 1.11 | 1.16 | 1.21 |
|---|---|---|---|---|---|---|---|---|---|---|---|---|---|---|
| $\omega_{4n0}/\omega \rightarrow$ | 0.38 | 0.39 | 0.40 | 0.41 | 0.42 | 0.43 | 0.44 | 0.45 | 0.46 | 0.47 | 0.48 | 0.49 | 0.50 | 0.51 |
| $kA$=0.10 | NO | NO | NO | NO | NO | NO | NO | YES* | NO | NO | NO | NO | NO | NO |
| $kA$=0.15 | NO | NO | NO | NO | NO | YES* | YES* | YES* | YES | YES | YES | YES | YES | YES |
| $kA$=0.20 | NO | NO | NO | YES* | YES | YES | YES | YES | YES | YES | YES | YES | YES | YES |
| $kA$=0.25 | YES | YES | YES | YES | YES | YES | YES | YES | YES | YES | YES | YES | YES | YES |

corresponding equally-steep shorter waves, so they can exceed more easily the local freeboard. The water shipping for the cases with 'YES*' are caused by the parametric roll, while the wave-body interactions do not lead to water on deck before the instability. It means that these events are dominated by large roll motions while those indicated with 'YES' are governed by heave and pitch motions. In terms of water-on-deck severity, the maximum nondimensional volume of shipped water per event $Q/(S_dA)$, with $S_d$ the deck area, is nonlinearly dependent on the wave steepness and largest around $\omega_{4n0}/\omega = 0.48$, see left plot of figure 12. The empty symbols in the figure give $Q/(S_dA)$ for steady-state water shipping events before parametric roll excitation. When the instability is excited by the shortest waves the water-on-deck severity is greatly increased with respect to the water-on-deck events before instability (compare the full symbols with the corresponding empty symbols). As the wavelength reduces, also the parametric-roll amplitude decreases and the instability effect in increasing the volume of water becomes more and more limited.

A larger amount of shipped water leads to larger green-water induced pressure on the deck. This is examined in the right panels of figure 12 for the case highlighted by the ellipse in the left plot. There, the top panel gives the pressure evolution predicted at locations 3 and 6 defined in the top-right sketch of figure 1. The bottom panel shows the corresponding roll evolution. Comparing them, it is clear that the instability largely increases the pressure level,

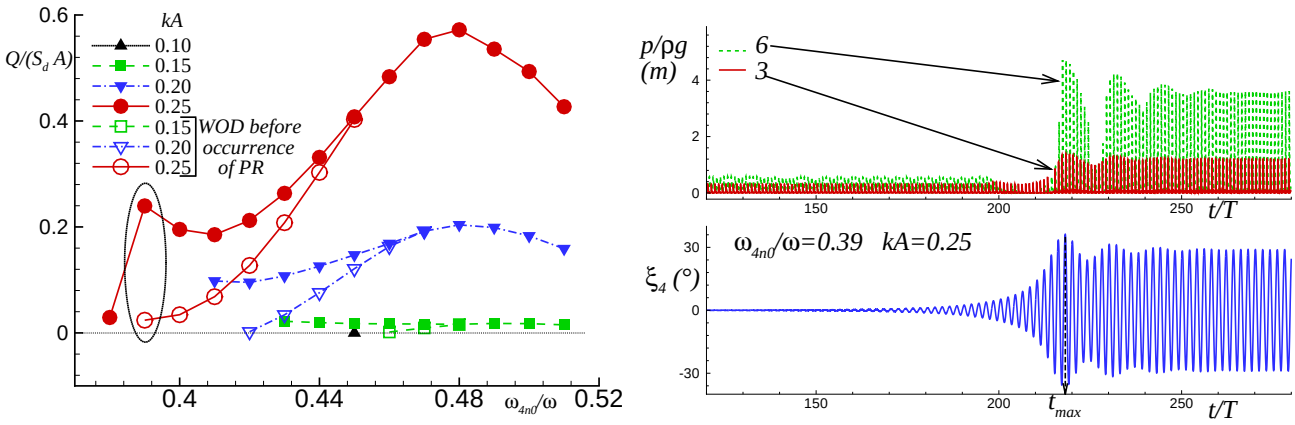


Figure 12: Influence of parametric roll on water on deck from numerical analysis. Left: maximum volume of shipped water $Q$ in steady-state conditions. $Q$ is made nondimensional by $S_d A$, with $S_d$ the deck area and $A$ the incident-wave amplitude, and is plotted for each examined steepness $kA$ as a function of the ratio between the calm-water roll natural frequency and the incident-wave frequency, $\omega_{4n0}/\omega$. Right: evolution of the deck pressure at sensors 3 and 6 in the top-right sketch of figure 1 (top) and of the roll motion (bottom). For the pressure, the values of the corresponding water-column height are given at full scale.

especially near the superstructure.

So far, we have investigated the effect of parametric roll on the water shipping but also the water-on-deck occurrence can affect the onset and features of roll instability because it leads to a variation of the roll added moment and roll damping, and modifies the location of the center of gravity of the vessel. The importance of these changes depends on the severity and features of the water shipping and is examined next.

Table 4 considers only the incident-wave cases leading to both parametric-roll and water-on-deck occurrences and provides qualitative information of the influence of water shipping on the roll instability. Such information were

Table 4: Influence of water on deck on parametric roll from numerical analysis: variation of $t_{max}$ and of steady-state amplitude when green-water loads are switched off in the simulations of the cases in tables 2 and 3 with both parametric roll (PR) and water on deck (WOD). A=PR avoided; D=delay in PR occurrence, *i.e.* longer transient phase; F=faster PR occurrence; S=same duration of transient phase as when accounting for WOD loads; U=(almost) unchanged steady-state amplitude (SSA); H=higher SSA; L=lower SSA.

| $\lambda/L \rightarrow$ | 0.70 | 0.74 | 0.78 | 0.82 | 0.86 | 0.90 | 0.94 | 0.98 | 1.02 | 1.07 | 1.11 | 1.16 | 1.21 |
|---|---|---|---|---|---|---|---|---|---|---|---|---|---|
| $\omega_{4n0}/\omega \rightarrow$ | 0.39 | 0.40 | 0.41 | 0.42 | 0.43 | 0.44 | 0.45 | 0.46 | 0.47 | 0.48 | 0.49 | 0.50 | 0.51 |
| 0.10 | | | | | | | SU | | | | | | |
| 0.15 | | | | | SU | SU | SU | DU | DH | | | | |
| 0.20 | | | SU | DL | FL | FL | FL | FL | A | | | | |
| 0.25 | FL | FL | FL | FL | FL | DL | A | | | | | | |

obtained by simulating these cases again but setting to zero the green-water loads $\boldsymbol{F}_{\text{wod}}$ in the equation of motion (1) and then checking the effect on parametric roll occurrence and features. The results indicate that the water on

deck is not able to affect the parametric roll when the water shipping itself is caused by the instability. Switching off $\boldsymbol{F}_{\text{wod}}$ leads to faster parametric roll but with lower amplitude in most of the cases, as the frequency ratio increases the transient phase becomes longer than when accounting for the green-water loads and the amplitude can be lower, unchanged or larger. It is important to note that in two cases, when avoiding $\boldsymbol{F}_{\text{wod}}$, the parametric roll does not occur. This means that the water shipping and its influence on the motions are responsible for the instability.

The quantitative importance of the water on deck is examined in figure 13 in terms of variation of $t_{max}$, *i.e.* $\Delta t_{max}$, and steady-state amplitude, *i.e.* $\Delta\xi_{4a}$, when the green-water loads are switched off. From the studied cases, the largest

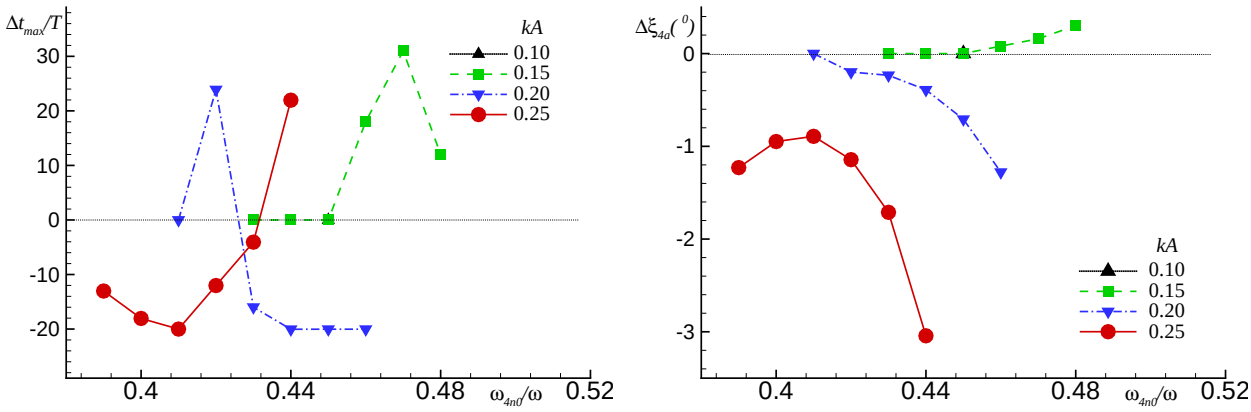


Figure 13: Influence of water on deck on parametric roll from numerical analysis: variation of the time required for the first roll peak (left) and of the steady-state roll amplitude (right) when the green-water loads are set to zero, *i.e.* $\Delta t_{max} = t_{maxNOWOD} - t_{maxWOD}$ and $\Delta\xi_{4a} = \xi_{4aNOWOD} - \xi_{4aWOD}$. The variables are plotted for each examined steepness $kA$ as a function of the ratio between the calm-water roll natural frequency and the incident-wave frequency $\omega_{4n0}/\omega$. $T$ is the incident-wave period.

variation in terms of duration of the transient phase is about $31T$, while the amplitude change is at most three degrees. However, if we examine the two cases where green-water loads are responsible for parametric roll, we find that the influence on roll amplitude is larger. The incident-wave parameters for these cases are, respectively, $\omega_{4n0}/\omega = 0.45$ and $kA$=0.25 and $\omega_{4n0}/\omega = 0.47$ and $kA$=0.20 and when water shipping is accounted for the parametric roll occurs, respectively, with $t_{max} \simeq 184T$ and $\xi_{4a} \simeq 7°$ and with $t_{max} \simeq 328T$ and $\xi_{4a} \simeq 6°$. The second of them has a very long transient phase but in practice a perturbation of the system could shorten the time for the excitation. This is examined in figure 14 showing the roll evolution when a Gaussian roll moment centered at $t = 10T$ and with a duration of about $0.02T$ is applied to the ship free in heave, pitch and roll. The maximum value of this moment would lead to a maximum roll of 5° or 1° when the ship is modelled as a 1-dof system. When water-on-deck loads are included in the motion equations the parametric roll is excited quicker by the two perturbations than without them and the steady-state roll amplitude is the same as without perturbation. If these loads are not accounted for, even the largest perturbation is not able to give a steady-state parametric roll and after a transient the roll damps out.

The effect of the water shipping on the transient phase could be relevant when group of waves, more than regular waves, interact with the vessel. Unluckily in this context water shipping occurrence can either increase or reduce the

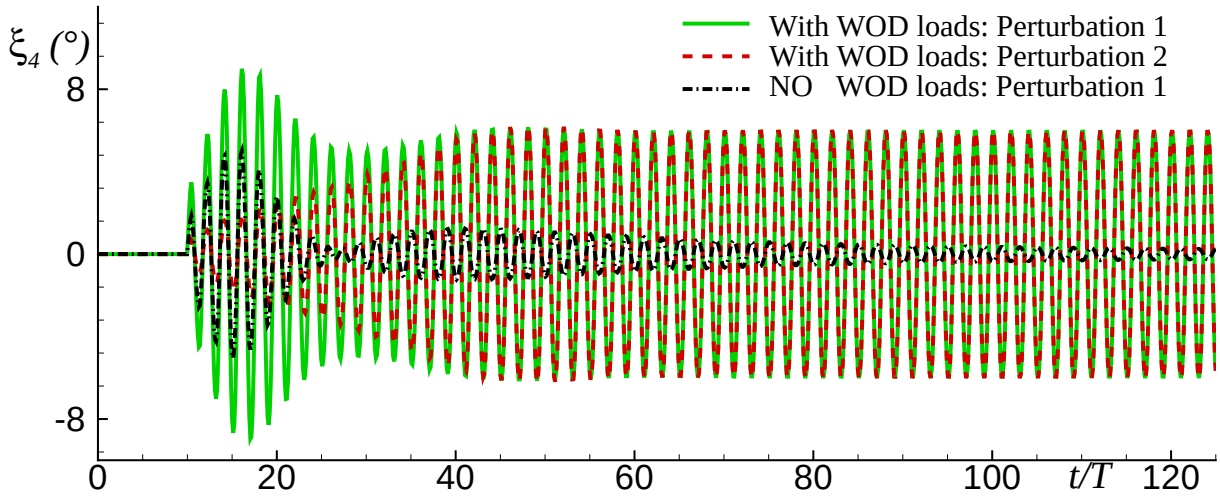


Figure 14: Influence of water on deck on parametric roll from numerical analysis: incident waves with $\omega_{4n0}/\omega = 0.47$ and $kA$=0.20. Roll evolution when a Gaussian roll moment centered at $t = 10T$ and with a duration of about $0.02T$ is applied to the ship free in heave, pitch and roll. The maximum value of the moment would lead to a maximum roll of 5° (Perturbation 1) or 1° (Perturbation 2) when the ship is modelled as a 1-dof system.

transient phase, depending on the steepness and the frequency ratio. It means that it is hard to make any suggestion about what is helpful for avoiding parametric roll. The results also show that once the parametric roll is established then the oscillation amplitude is not much affected by water on deck. In this context the relative importance increases as the instability is by itself not much pronounced (compare the right plot of figure 13 with the right plot of figure 11).

From practical point of view, it is important to try to find the proper scaling parameters governing the variation of the transient phase and of the roll amplitude induced by water on deck. These variables are defined as opposite to those given in figure 13, *i.e.* positive values mean, respectively, longer transient phase and larger roll amplitude due to water shipping. They are plotted in figure 15 in terms of parameters $\alpha = -\Delta t_{max}/(T \cdot \epsilon) \cdot 10^{-4}$ and $\gamma = -\Delta\xi_{4a}/\epsilon$, respectively, as a function of $\delta = 10(\omega/\omega_{4n0})^2 \cdot \epsilon$. All numerical results for the examined steepnesses $kA$ seem to follow a clear trend for each variable of interest. The results identify the modified steepness $\epsilon = (2A - f)/\lambda$, with $f$ the ship mean freeboard, as an important parameter of the problem. This has been already pointed out in [11] and in [5] for variables connected with water on deck, in the context of incident wave packets and regular waves, respectively. Please note that $\epsilon$ has both negative and positive values for the examined cases. A negative value means that the incident-wave height is smaller than the mean freeboard so water shipping is possible due to the body motions and to the radiation and diffraction effects of the vessel. Both the parameter connected with the variation of the transient-phase duration and the one related with the variation of the roll steady-state amplitude involve a division by $\epsilon$ and so they are singular when $2A = f$. As expected both $\alpha$ and $\gamma$ vary more rapidly going from positive $\epsilon$ to zero than going from negative $\epsilon$ to zero. This is because for positive $\epsilon$ the incident waves will exceed more easily the freeboard and then cause more pronounced water shipping. The latter has in return greater chance to affect the parametric roll. The

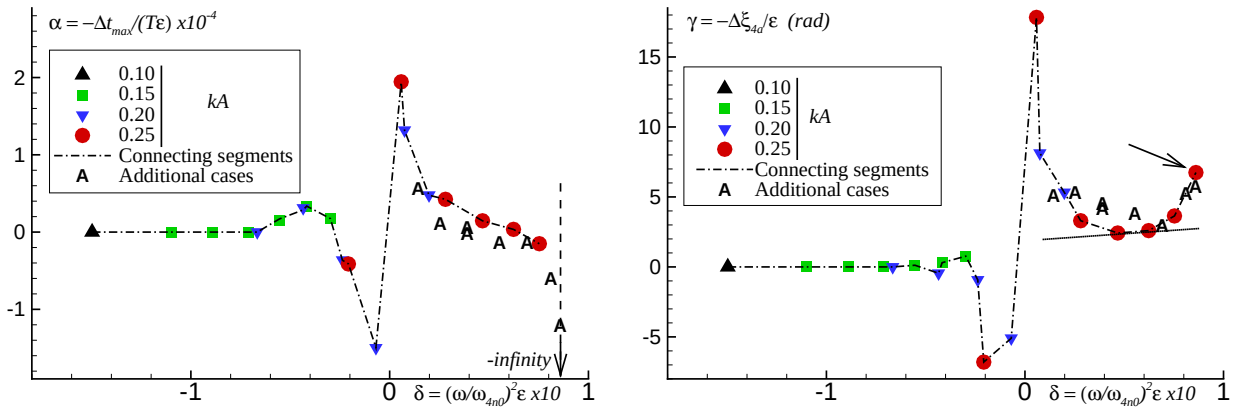


Figure 15: Influence of water on deck on parametric roll from numerical analysis: scaling laws for the variation of $t_{max}$ (left) and of $\xi_{4a}$ (right) caused by the green-water loads, *i.e.* $-\Delta t_{max} = t_{maxWOD} - t_{maxNOWOD}$ and $-\Delta\xi_{4a} = \xi_{4aWOD} - \xi_{4aNOWOD}$. The modified steepness $\epsilon$ defined as $(2A - f)/\lambda$ is involved. $A$, $T$ and $\lambda$ are the incident-wave amplitude, period and wavelength, respectively, and $f$ the ship mean freeboard. The dotted segment in the right plot is parallel to $y = \delta$.

most relevant range of $\delta$ is for positive and increasing values. In this case, $\alpha$ tends to decrease and become negative, *i.e.* shorter transient phase with water shipping; $\gamma$ reaches a minimum and then tends to increase quicker than $\delta$ (the dotted segment in the right plot of the figure is parallel to $y = \delta$). This means that for large $\delta$, the increase of roll amplitude due to water shipping rises more than linearly with $\epsilon$ for constant frequency ratio.

The discussed scaling laws concern cases where the parametric roll is excited both without and with accounting for the water-shipping loads in the motion equations. However, it is interesting to note that the results for one of the cases where parametric roll is caused by water on deck ($\omega_{4n0}/\omega = 0.45$ and $kA$=0.25) seem to be consistent with the trends for large and increasing $\delta$. These results are also reported in figure 15 and indicated by the arrow in each plot. They correspond to a variation of $t_{max}$ equal to $-\infty$ because without green-water loads there would be no parametric roll at all. This is always the case when the parametric roll is associated with the water shipping and so, strictly speaking, the variation in the transient phase does not have much meaning. The variation of $\xi_{4a}$ is equal to the steady-state roll amplitude when accounting for the water-on-deck loads. The other incident-wave case where parametric roll is caused by water on deck ($\omega_{4n0}/\omega = 0.47$ and $kA$=0.2) does not satisfy these scaling laws (not shown in the figure).

To check the goodness of the scaling laws in the relevant zone of positive and increasing $\delta$, additional cases were studied numerically by varying the incident-wave steepness and the frequency ratio as reported in table 5, so to have parametric roll and water on deck. The corresponding results are indicated by symbols 'A' in figure 15. The new data

Table 5: Steepness and frequency ratio for each of the eight additional incident-wave cases studied numerically.

| $(kA, \omega_{4n0}/\omega)$ | | | | | | | |
|---|---|---|---|---|---|---|---|
| (0.2, 0.465) | (0.22, 0.45) | (0.234, 0.445) | (0.25, 0.435) | (0.25, 0.445) | (0.253, 0.445) | (0.2085, 0.445) | (0.217, 0.454) |

are close to the others but there are some visible differences. This motivated a further check of the proper scaling laws

and new parameters, $\alpha 1 = -(\Delta t_{max}/T)\cdot\epsilon$, $\gamma 1 = -10\Delta\xi_{4a}\cdot\epsilon$ and $\delta 1 = 100(\omega_{4n0}/\omega)^2\cdot\epsilon$, were identified as documented in figure 16. In this case there is some scattering for the variation of the transient phase, but it is localized in the

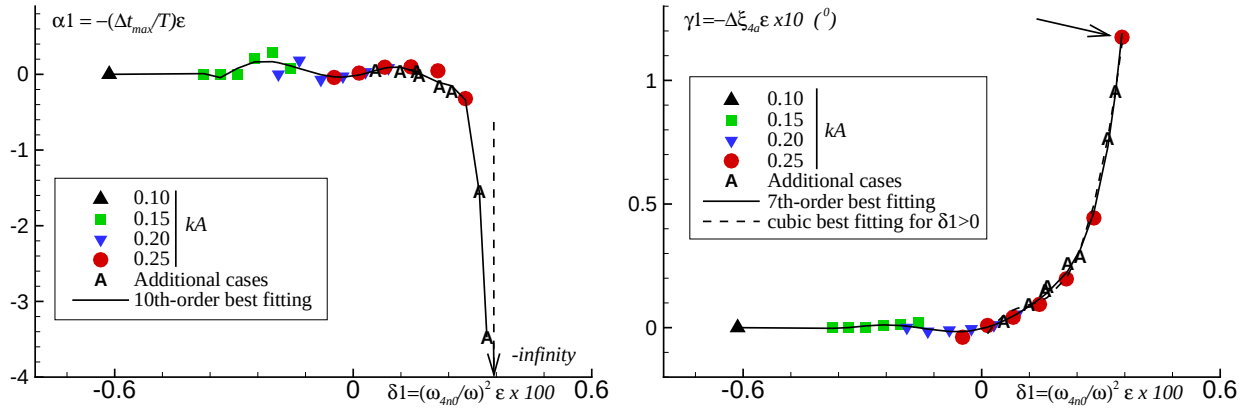


Figure 16: Influence of water on deck on parametric roll from numerical analysis: scaling laws for the variation of $t_{max}$ (left) and of $\xi_{4a}$ (right) caused by the green-water loads, *i.e.* $-\Delta t_{max} = t_{maxWOD} - t_{maxNOWOD}$ and $-\Delta\xi_{4a} = \xi_{4aWOD} - \xi_{4aNOWOD}$. The modified steepness $\epsilon$ defined as $(2A - f)/\lambda$ is involved. $A$, $T$ and $\lambda$ are the incident-wave amplitude, period and wavelength, respectively, and $f$ the ship freeboard. For $\alpha 1$, the best fitting is obtained using a 10th-order polynomial with a mean square-root error $er \simeq 0.0624$ and results $\alpha 1 = (-1.8652\delta 1^{10} - 1.8473\delta 1^9 - 0.2137\delta 1^8 + 0.2452\delta 1^7 + 0.0717\delta 1^6 - 0.0048\delta 1^5 - 0.0052\delta 1^4 - 0.0004\delta 1^3 + 0.0001\delta 1^2)\cdot 10^5$. For $\gamma 1$, the best fitting is obtained using a 7th-order polynomial with $er \simeq 0.0159$ and results $\gamma 1 = 358.784\delta 1^7 + 355.769\delta 1^6 + 41.668\delta 1^5 - 33.274\delta 1^4 - 0.408\delta 1^3 + 3.427\delta 1^2 + 0.397\delta 1 - 0.005$. The cubic polynomial best-fitting is also reported for $\gamma 1$ for positive $\delta 1$. This corresponds to $\gamma 1 = 70.192\delta 1^3 - 24.122\delta 1^2 + 3.213\delta 1 - 0.067$ with $er \simeq 0.0286$.

region of negative $\delta 1$, where the variation of $t_{max}$, as well as of $\xi_{4a}$, due to water shipping is very limited. The new scaling laws are better in the zone with greater influence of water on deck. With the present choice of the parameters, single polynomial best-fitting can be obtained for $\alpha 1(\delta 1)$ and $\gamma 1(\delta 1)$ because both of them are regular functions of $\delta 1$. In the figure, a 10th-order polynomial with a mean square-root error $er \simeq 0.0624$ and a 7th-order polynomial with $er \simeq 0.0159$ are proposed, respectively. For the parameter $\gamma 1$, associated with the variation of the steady-state amplitude, a cubic polynomial best-fitting could be used in the relevant range $\delta 1 > 0$ with $er \simeq 0.0286$. This is documented in the right plot of figure 16. The variation of the transient phase needs instead higher-order polynomial best-fitting also when considering $\delta 1 > 0$ (at least fifth-order). The proposed polynomial curves in figure 16 could be useful to estimate the variations of $t_{max}$ and $\xi_{4a}$ due to water shipping for other incident-wave parameters.

## 5. Conclusions

A combined numerical and experimental investigation has been carried out on the occurrence of parametric roll and water on deck on a FPSO ship in head-sea regular waves. The numerical solver uses a Domain-Decomposition strategy coupling: a weakly-nonlinear potential-flow seakeeping solver based on the weak-scatterer theory, a shallow-water approximation of the water flowing onto the deck for global dam-breaking type of water shipping, and a Wagner-type bottom-slamming model. The physical investigation has been focused on the occurrence and features of roll instability

and water on deck. The two phenomena were studied varying the incident-wave parameters and their mutual influence has been examined. The solver provides results globally consistent with the experiments, with a good agreement in terms of motion amplitudes, in particular for the roll. The major discrepancies in terms of phenomena occurrence are documented for cases more sensitive to the involved nonlinearities and so to the numerical approximations. For the steepness range examined, the instability occurs at $\omega_{4n0}/\omega < 0.52$ and is affected by nonlinear effects in the wave-body interactions. More in detail, for sufficiently short waves, increasing the incident-wave steepness $kA$ tunes the actual roll natural period to be twice the incident-wave period and so excites the parametric resonance. Larger values of $kA$ bring out from the instability for longer waves. This is an important aspect because it implies a wider region of parametric roll toward shorter waves. The parametric roll generally increases the water shipping severity in terms of amount of shipped water and of green-water loads on the deck and can even be direct responsible of the water on deck. Concerning the key question of present work: the water shipping affects in return the parametric roll and in general tends to increase the roll amplitude, up to about seven degrees for the examined cases. It can either enlarge or shorten the transient phase. A scaling analysis has been proposed for the variation of the duration of the transient phase and of the steady-state amplitude of the parametric roll induced by water shipping. The results identify the modified steepness $\epsilon = (2A - f)/\lambda$ as an important parameter. The scaling laws $\alpha 1(\delta 1)$ and $\gamma 1(\delta 1)$ appeared to be more suitable than $\alpha(\delta)$ and $\gamma(\delta)$ in the region where water shipping is more relevant for parametric roll. They are well approximated by polynomial curves which could be useful to estimate the variations of $t_{max}$ and $\xi_{4a}$ due to water shipping for incident-wave parameters different from those examined here.

**Acknowledgment**

This research activity is partially funded by the Centre of Excellence CeSOS, NTNU, Norway, partially by the Research Council of Norway through the Centres of Excellence funding scheme AMOS, project number 223254, and partially by the Flagship Project RITMARE - The Italian Research for the Sea - coordinated by the Italian National Research Council and funded by the Italian Ministry of Education, University and Research within the National Research Program 2011-2013.

**References**

[1] O. M. Faltinsen, Hydrodynamics of High-Speed Marine Vehicles, Cambridge University Press, Cambridge, UK, 2005.

[2] M. Greco, C. Lugni, Numerical and experimental study of parametric roll with water on deck, in: Proc. of Int. Conference on Violent Flows (VF-2012), Nantes, France, 2012.

[3] M. Greco, C. Lugni, 3-d seakeeping analysis with water on deck and slamming. part 1: numerical solver, Journal of Fluids and Structures 33 (2012).

[4] H. Wagner, Uber stoss- und gleitvorgange an der oberflache von flussigkeiten, ZAMM 12 (1932) 192–235.

[5] M. Greco, G. Colicchio, O. M. Faltinsen, Shipping of water on a two-dimensional structure. part 2, Journal of Fluid Mechanics 581 (2007) 371–399.

[6] G. Colicchio, Violent disturbance and fragmentation of free surfaces, Ph.D. thesis, University of Southampton, Southampton, UK, 2004.

[7] J. Pawlowski, A theoretical and numerical model of ship motions in heavy seas, in: SNAME Transactions, volume 99, 1991, pp. 319–315.

[8] W. Cummins, The impulse response function and ship motions, Symposium on Ship Theory, Schiffstechnik 9 (1962) 101–109.

[9] Y. Kawahara, K. Maekawa, Y. Ikeda, A simple prediction formula of roll damping of conventional cargo ships on the basis of ikedas method and its limitation, in: Proc. 10th Intl. Conf. on Stability of Ships and Ocean Vehicles, St. Petersburg, Russia, 2009.

[10] M. Greco, B. Bouscasse, C. Lugni, 3-d seakeeping analysis with water on deck and slamming. part 2: Experiments and physical investigation, Journal of Fluids and Structures (2012).

[11] M. Barcellona, M. Landrini, M. Greco, O. Faltinsen, An experimental investigation on bow water shipping, Journal Ship Research 47 (2003) 327–346.